IEEE Trans. Microwave Theory Tech., vol. MTT-20, pp. 497–504, Aug. 1972.
[5] P. Benedek and P. Silvester, "Capacitance of parallel rectangular plates separated by a dielectric sheet," *IEEE Trans. Microwave Theory Tech.*, vol. MTT-20, pp. 504–510, Aug. 1972.
[6] A. Gopinath, B. Easter, and R. Horton, "Microstrip loss calculations," *Electron. Lett.*, vol. 6, pp. 40–42, 1970.
[7] E. J. Denlinger, "A frequency dependent solution for microstrip transmission lines," *IEEE Trans. Microwave Theory Tech.*, vol. MTT-19, pp. 30–39, Jan. 1971.
[8] P. Silvester, "Skin effect in multiple and polyphase conductors," *IEEE Trans. Power Appl. Syst.*, vol. PAS-88, pp. 231–238, May 1969.
[9] Z. Csendes, A. Gopinath, and P. Silvester, "Generalised matrix inverse techniques for local approximations of operator equations," in *Mathematics of Finite Elements and its Applications*, J. Whiteman, Ed. New York: Academic, to be published.

Effect of Upper Sideband Impedance on a Lower Sideband Up-Converter

W. ALAN DAVIS AND PETER J. KHAN

***Abstract*—An analysis is given of a lower sideband up-converter which includes a finite circuit reactance X_{33} at the upper sideband frequency, in addition to the circuit impedances at the input signal and output lower sideband frequencies.**

The expressions developed for the gain, gain sensitivity to pump power variation, and noise figure show the extent to which gain and gain sensitivity decrease, and noise figure increases when X_{33} is finite, as compared to the case when X_{33} is infinite. For a simple circuit configuration the gain–bandwidth product changes markedly when X_{33} is small at the center frequency. In addition, when second-harmonic pump power is allowed to flow through the varactor diode, the performance of the lower sideband up-converter can be improved.

I. Introduction

The lower sideband up-converter (LSUC) has been shown to have significant advantages over the reflection-type amplifier for low-noise receiver applications [1]. These advantages include a greater gain–bandwidth product, reduced gain sensitivity to pump power variations (at the expense of a very slight increase in noise figure and an output at an elevated frequency which limits input to low microwave frequencies), and elimination of the need for a circulator, which is also advantageous in cryogenic or miniaturized applications.

A significant problem in LSUC design has been the propagation of the upper sideband frequency; this is usually undesirable because power dissipation at this frequency in the diode and in the circuit resistances gives rise to degenerative feedback. A consequence is that the resulting induced positive resistance in the signal circuit subtracts from the parametrically generated negative resistance and reduces the gain.

Several authors have considered analytically the effect of upper sideband propagation in an LSUC. However, in most cases these authors have used a representation of the reverse-biased varactor-diode equivalent circuit consisting of a resistance and a variable capacitance in parallel [2], [3] or a lossless capacitance [4]. Although this simplifies the mathematics considerably, it yields significant inaccuracy when applied to multisideband circuits, since it leads to the erroneous conclusion that power dissipation in the diode can be avoided at harmonic sideband frequencies by the presence of a short circuit connected across the diode terminals. A more accurate approach, based upon matrix manipulation, has been used by Ernst [5] and by Howson and Smith [6], who carry out a general analysis of a multiple-sideband parametric network, using a diode representation consisting of a resistance in series with the variable capacitance. However, the work of Ernst is restricted to parametric amplifiers, while Howson and Smith consider only the multisideband converter having an output at the upper sideband frequency.

In most practical LSUC's, the upper sideband and the harmonic-sideband circuits consist of the diode series resistance R_s together with a reactance determined by the diode mount structure and the position of the pump, signal input, and lower sideband output filters. Loading of these sidebands with any resistance other than that resulting from the diode, transmission line, or filter losses is attainable only at the expense of considerable increase in circuit complexity.

This paper is concerned with the effect of upper sideband propagation on LSUC performance for the case where R_s is the only resistance in the upper sideband circuit. The study was motivated by the desire to answer the following two questions which arise in LSUC circuit design.

1) Over what range of values of the upper sideband circuit reactance X_{33} will the propagation of the upper sideband exert a negligible effect upon the operating performance of an LSUC which has been designed without considering the upper sideband?

2) Propagation of the upper sideband is known to provide a decrease in transducer power gain and in the gain sensitivity to pump power variations; this reduction in gain sensitivity is desirable for some applications. What is the extent of the increase in noise figure resulting from this upper sideband

Manuscript received August 21, 1972; revised January 29, 1973. This work was supported by the U. S. Army Electronics Command, Fort Monmouth, N. J., under Contract DAAB-07-68-C-0138.
W. A. Davis was with the Cooley Electronics Laboratory, Department of Electrical and Computer Engineering, University of Michigan, Ann Arbor, Mich. 48105. He is now with the Communications Research Laboratory, Department of Electrical Engineering, McMaster University, Hamilton, Ont., Canada.
P. J. Khan is with the Cooley Electronics Laboratory, Department of Electrical and Computer Engineering, University of Michigan, Ann Arbor, Mich. 48105.

propagation, and what is the effect upon gain–bandwidth product?

When frequency-sensitive calculations are performed in this paper, the LSUC circuit is restricted to having a relatively simple diode model in which parasitic packaging and mounting elements are neglected and have input and output ports which are single-tuned lumped elements. Nevertheless, in these cases the results obtained provide a fundamental indication of the performance to be expected in a practical microwave circuit.

II. Equivalent-Circuit Formulation

Analysis of multisideband frequency converters usually leads to a mass of algebraic expressions with a resulting loss of physical insight. This loss can be partially avoided through use of an equivalent-circuit representation.

The pumped varactor diode is assumed to be coupled through bandpass filters to LSUC input and output circuits having impedances R_g+jX_1 and R_l+jX_2, respectively, and to an upper sideband circuit having an impedance jX_3. The pumped diode elastance S is expressed by

$$S = \sum_{n=-\infty}^{\infty} S_n e^{jn\omega_p t}$$

for a pump frequency $f_p=\omega_p/2\pi$.

If the circuit contains externally applied voltages V_1, V_2, and V_3 at the signal frequency f_1 and at both lower and upper sideband frequencies f_2 and f_3, respectively, the relationship between these voltages and the corresponding current components at these three frequencies is readily obtained using standard means [7].

$$\begin{bmatrix} V_1 \\ V_2{}^* \\ V_3 \end{bmatrix} = \begin{bmatrix} Z_{11} & \dfrac{jS_1}{\omega_2} & \dfrac{-jS_1}{\omega_3} \\ \dfrac{-jS_1}{\omega_1} & Z_{22}{}^* & \dfrac{-jS_{-2}}{\omega_3} \\ \dfrac{-jS_1}{\omega_1} & \dfrac{jS_2}{\omega_2} & Z_{33} \end{bmatrix} \cdot \begin{bmatrix} i_1 \\ i_2{}^* \\ i_3 \end{bmatrix} \quad (1)$$

where

$$Z_{11} = R_g + R_s + jX_1 - jS_0/\omega_1$$
$$Z_{22} = R_l + R_s + jX_2 - jS_0/\omega_2$$
$$Z_{33} = R_s + jX_3 - jS_0/\omega_3.$$

The time origin has been chosen so that $S_1=S_{-1}$, and the circuit is assumed to present an open circuit when viewed from the diode junction terminals at all sideband frequencies greater than ω_3. Circuit characterization in the form expressed in (1) is for noise figure determination carried out in Section VI. However, for determination of gain properties, the circuit may be regarded as a two-port network by setting the externally applied V_3 equal to zero.

The circuit equation then reduces to

$$\begin{bmatrix} V_1 \\ V_2{}^* \end{bmatrix} = \begin{bmatrix} Z_{11}' & Z_{12}' \\ Z_{21}' & Z_{22}' \end{bmatrix} \begin{bmatrix} I_1 \\ I_2{}^* \end{bmatrix} \quad (2)$$

where * indicates complex conjugate and

$$Z_{11}' = Z_{11} + \frac{X_{31}X_{13}}{Z_{33}} \quad (3a)$$

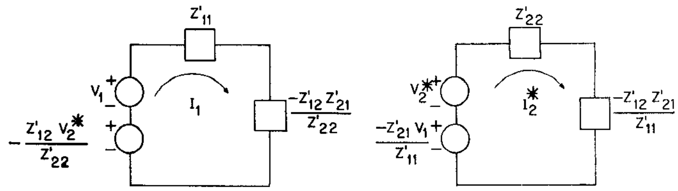

Fig. 1. General equivalent circuit at the input and output of the LSUC.

$$Z_{12}' = jX_{12} - \frac{X_{13}X_{32}}{Z_{33}} \quad (3b)$$

$$Z_{21}' = -jX_{21} + \frac{X_{23}X_{31}}{Z_{33}} \quad (3c)$$

$$Z_{22}' = Z_{22}{}^* - \frac{X_{32}X_{23}}{Z_{33}}. \quad (3d)$$

The off-diagonal terms in the impedance matrix in (1) have been represented by jX_{12}, $-jX_{13}$, etc.

The effect of the upper sideband circuit appears in the presence of the second term in each of the four equations (3a)–(3d). It is noteworthy that each of these additional terms contains both resistive and reactive components.

Using (2) a general equivalent circuit is derived in the form shown in Fig. 1. It is evident from this circuit that the coupling between input and output circuits through the pumped diode is represented by the induced impedances $(-Z_{12}'Z_{21}')/Z_{22}'$ and $(-Z_{12}'Z_{21}')/Z_{11}'$ and by the transformed voltage components $(-Z_{12}'V_2{}^*)/Z_{22}'$ and $(-Z_{21}'V_1)/Z_{11}'$. Using (3a) Z_{11}' may be written in the form

$$Z_{11}' = Z_{11} + \Delta R_{11} - j\Delta X_{11}$$

where

$$\Delta R_{11} = R_s\left(\frac{X_{13}X_{31}}{R_s{}^2 + X_{33}{}^2}\right)$$

$$\Delta X_{11} = \frac{X_{33}X_{31}X_{13}}{R_s{}^2 + X_{33}{}^2}$$

and

$$Z_{33} = R_s + jX_{33}.$$

These additional components in Z_{11}' arise through the double-conversion process $\omega_1 \rightarrow \omega_3$ followed by $\omega_3 \rightarrow \omega_1$; the resistance in the signal circuit is augmented by the positive component ΔR_{11}.

By contrast (3d) gives

$$Z_{22}' = Z_{22}{}^* - \Delta R_{22} + j\Delta X_{22}$$

where

$$\Delta R_{22} = R_s\left(\frac{X_{23}X_{32}}{R_s{}^2 + X_{33}{}^2}\right)$$

$$\Delta X_{22} = \frac{X_{33}X_{23}X_{32}}{R_s{}^2 + X_{33}{}^2}.$$

The resistive component induced in the output circuit is negative and diminishes Re (Z_{22}'). It arises from the double-conversion process $\omega_2 \rightarrow \omega_3$ and $\omega_3 \rightarrow \omega_2$ using the elastance variation

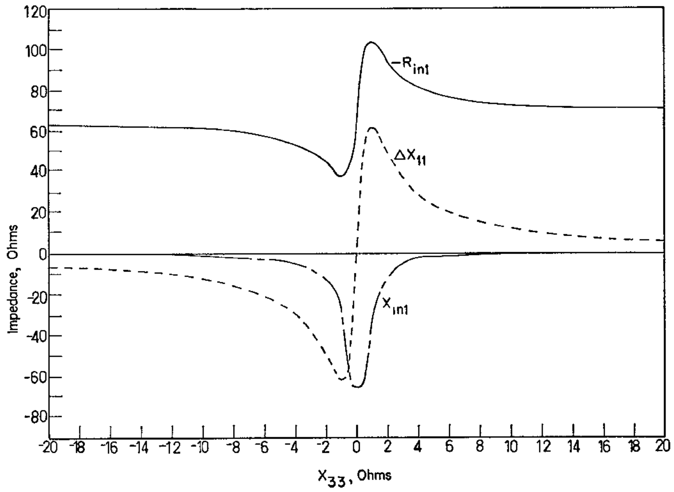

Fig. 2. LSUC input circuit parameters as a function of X_{33} for the up-converter of Table I.

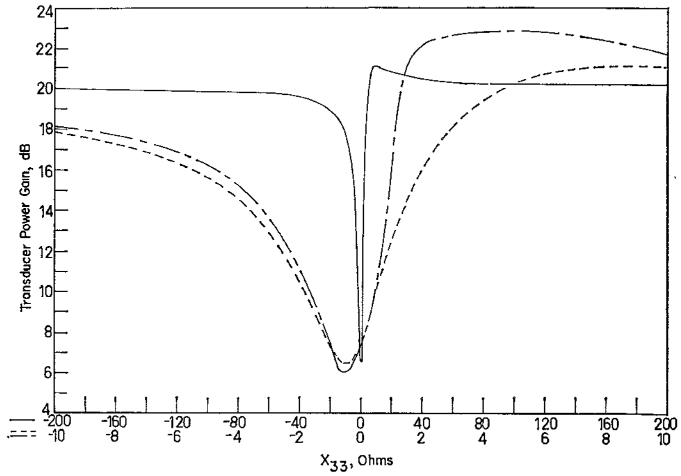

Fig. 3. Midband transducer power gain for the LSUC of Table I for passive tuning—two abscissa scales—(——, ---), and for hot tuning when input and output ports are loaded (—— -).

TABLE I

Parameters Used for the Lower Sideband Up-Converter

$1/S_0$	=	1.586 pF
S_1/S_0	=	0.35
S_2/S_0	=	0.044
S_{-2}	=	S_2
R_g	=	100 Ω
R_l	=	1.3 Ω
R_s	=	1.0 Ω
f_p	=	9.000 GHz
f_{10}	=	1.000 GHz

at $2\omega_p$ as a "pump"; since $\omega_3 = 2\omega_p - \omega_2$ the induced resistance is negative.

The additional component in Z_{12}' represents coupling from ω_1 to ω_2 by $\omega_1 \to \omega_3$ with a ω_p pump and $\omega_3 \to \omega_2$ with a $2\omega_p$ pump; similar remarks apply to Z_{21}'. It is evident from Fig. 1 that these additions affect the magnitude of the induced negative resistance in both input and output circuits.

Some insight into the effect of X_{33} upon these parameters may be found from Fig. 2 where the input circuit parameters ΔX_{11} and $Z_{in\,1} = (-Z_{12}'Z_{21}')/Z_{22}'$ are plotted as a function of X_{33} for an LSUC circuit shown in Table I. These parameters have been chosen to give 20-dB gain at resonance, when the effect of X_{33} is neglected. Fortunately, the large variation in these impedance values occurs over a small range of X_{33} near zero. Note that the induced negative resistance $-R_{in\,1}$ is plotted in this graph.

III. Effects of X_{33} on Gain

Impedance variations will of course affect the transducer power gain, which is given by

$$G_{21} = |Y_{21}|^2 4R_l R_g \quad (4)$$

where Y_{21} is the row-2 column-1 element of the inverse of (1). The expansion of this gain expression is given in Appendix I. When the second-harmonic power is negligible, i.e., $S_2 = 0$, the gain expression simplifies to

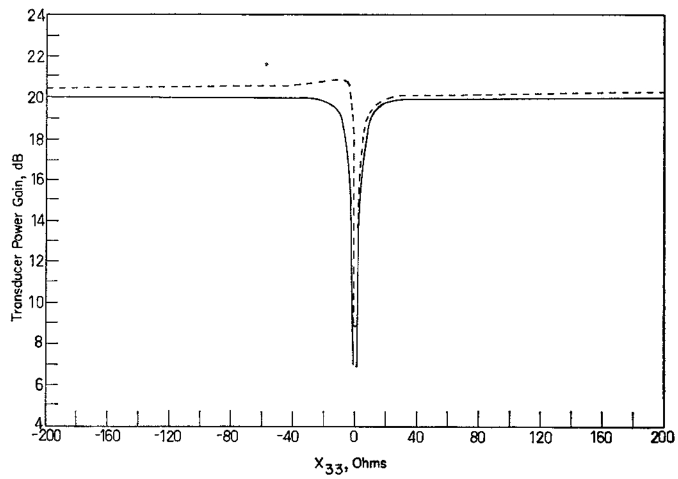

Fig. 4. The midband (——) and the maximum (----) gain when $S_2 = 0$ with passive tuning.

For a given pump power and load resistance, midband gain cannot be enhanced when X_{33} is finite and when $S_2 = 0$. The full expression in Appendix I shows that some increase in midband gain is possible when $S_2 \neq 0$.

The input and output impedances can be tuned with a single lumped element under the following three conditions: 1) S_0 resonated, corresponding to passive tuning; 2) S_0 and X_{11} (and X_{22} at ω_2) resonated, corresponding to hot tuning (applied pump power on) when the output or input ports, respectively, are open circuited; and 3) S_0, X_{11}, and Im ($Z_{in\,1}$) and the similar reactances at ω_2 are resonated, corresponding to hot tuning when input and output ports are loaded.

Under these tuning conditions the gain of the LSUC is examined as a) a function X_{33}, and b) a function of frequency. For case a) the gain given by (4) for the LSUC parameters listed in Table I under tuning conditions 1) and 3) above is plotted in Fig. 3 and shows a variation from 6 to 23 dB where

$$G_{21} = \frac{4R_g R_l |X_{21}|^2}{[(R_l + R_s)(R_g + R_s + \Delta R_{11}) - X_{12}X_{21}]^2 + [(R_l + R_s)\Delta X_{11}]^2}. \quad (5)$$

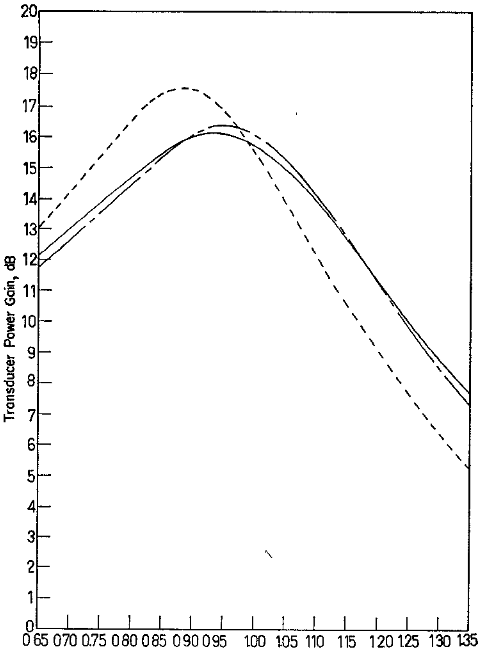

Fig. 5. Transducer power gain for LSUC of Table I when $X_{33} = -5\ \Omega$ at midband under three tuning conditions: passive tuning (----), hot tuning for open-circuited ports (—— -), and hot tuning for loaded ports (——).

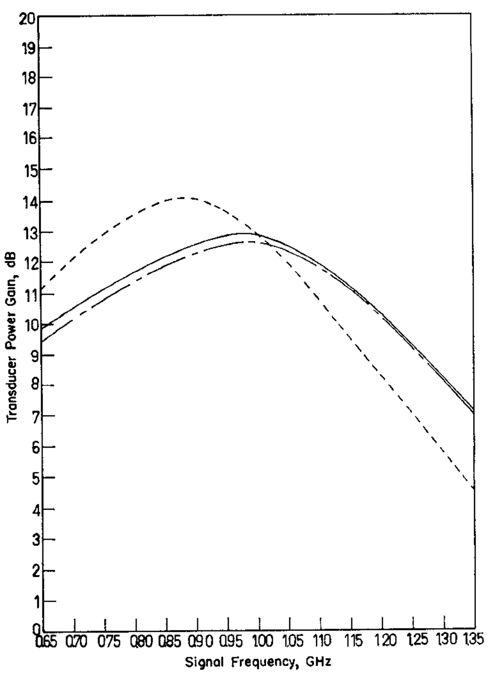

Fig. 6. Transducer power gain for the LSUC of Table I, except $S_2/S_0 = 0.1$ when $X_{33} = -5\ \Omega$ at midband under three tuning conditions: passive tuning (---), hot tuning for open-circuited ports (—— -), and hot tuning for loaded ports (——).

the design goal was 20 dB. Slightly wider variations occur under hot tuning conditions. When $S_2 = 0$, the midband gain curve shown in Fig. 4 is symmetrical about $X_{33} = 0$, although the nonresonant maximum gain, also plotted for this case, does exhibit a large gain for a small range of values of X_{33}.

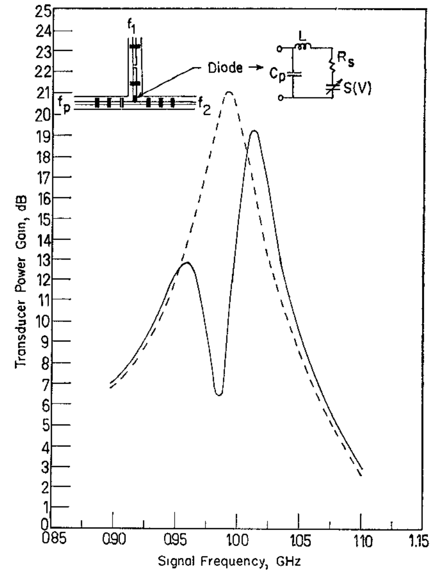

Fig. 7. Gain of an LSUC using coaxial microwave bandpass impedance transformers where the diode $R_s = 1\ \Omega$, lead inductance is 2 nH, diode package capacitance equals 0.5 pF, $f_p = 9.500$ GHz, $f_{10} = 1.000$ GHz, and other parameters given in Table I. Shown is the gain when $X_{33} = \infty$ (----), and the gain when upper sideband reactance is included (——).

For case b), where the gain is observed as a function of frequency for a fixed midband X_{33}, Figs. 5 and 6 show the gain for two separate values of second-harmonic elastance variation. Increasing S_2 clearly reduces the gain when X_{33} is small, while the effect of nonzero S_2 decreases as $|X_{33}|$ increases. Also, in all three tuning conditions, the maximum gain occurs below the midband frequency, as has been observed when X_{33} is infinite [8].

However, at microwave frequencies single-tuned lumped circuits are rarely available and a packaged varactor diode always has significant additional parasitic reactances. Consequently, an LSUC was analyzed which consisted of a packaged diode series mounted in a coaxial T junction with coaxial bandpass impedance transformers at each of the three ports. Because of the high-Q circuits involved in this more realistic model, a sharp dip occurs in the transducer power-gain curve (Fig. 7); this dip is completely missed when an approximate analysis is conducted (i.e., when the upper sideband reactance is assumed infinite). This demonstrates the importance of considering impedances at the higher sideband frequencies.

IV. Effects of X_{33} on Gain Sensitivity

One important source of gain instability in an LSUC is variation in the pump power source. Although the pump provides all the harmonic elastance coefficients $S_1, S_2, S_3, \cdots$, an approximate value of the gain sensitivity can be found by assuming that only the fundamental elastance coefficient is nonzero. The approximate gain sensitivity with respect to pump power is given by a sensitivity coefficient S_p defined as follows:

$$S_p = \frac{S_1^2}{G_{21}} \frac{\partial G_{21}}{\partial S_1^2} = 1 + \frac{S_1 G_{21}^{1/2}}{\omega_{20}(R_l R_g)^{1/2}} M_s \tag{6}$$

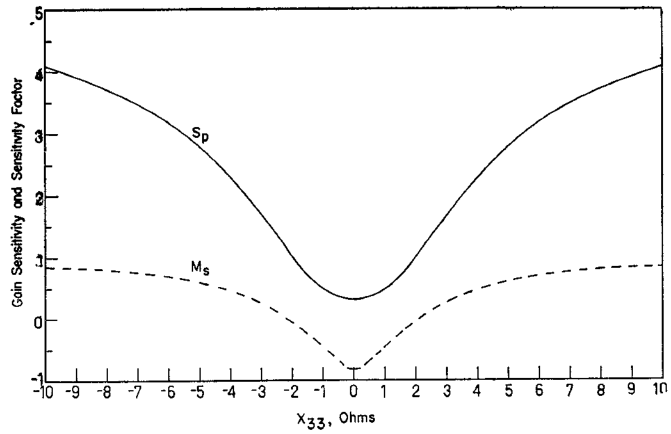

Fig. 8. Gain sensitivity for LSUC of Table I where $S_2=0$.

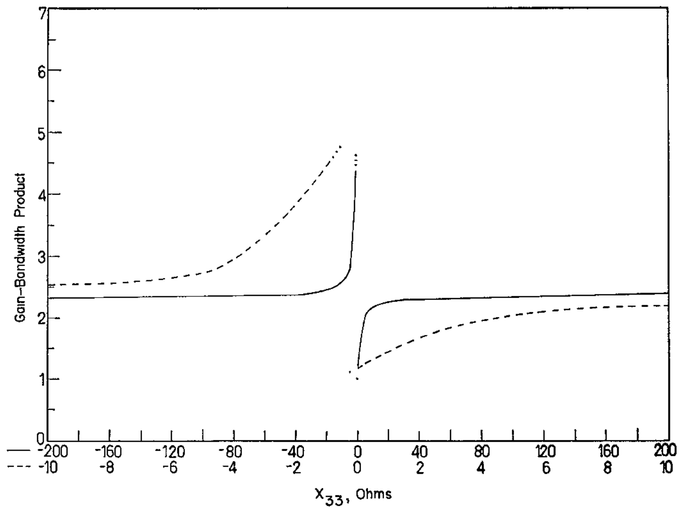

Fig. 9. Gain–bandwidth product ($G^{1/2}w$) for the LSUC of Table I.

where

$$M_s = \frac{X_{33}^2 M_e + M_f M_g}{[(R_s^2 + X_{33}^2)(X_{33}^2 M_e^2 + M_f^2)]^{1/2}}. \tag{7}$$

The factors M_e, M_f, and M_g, which are independent of X_{33}, are given in Appendix II. The value of the multiplying factor M_s is equal to one when $|X_{33}| = \infty$, but the gain sensitivity can be improved when X_{33} is finite, as shown in Fig. 8, although at the cost of lower gain (Fig. 4).

For a specified value of gain and X_{33}, the conditions for which the gain sensitivity can be improved by the finite value of X_{33}, i.e., when $M_s<1$ leads to restricting the lower sideband load resistance to be below a certain value. To find this value explicitly, an inequality is formed by setting the right side of (7) to be less than 1. After squaring this inequality and canceling the X_{33}^4 terms, the condition for improved gain sensitivity reduces to

$$0 < X_{33}^2(M_f^2 - 2M_eM_fM_g + M_e^2R_s^2) + M_f^2(R_s^2 - M_g^2).$$

The inequality $M_s<1$ is therefore satisfied if the coefficient of $X_{33}^2>0$ and $(R_s^2-M_g^2)>0$. However, both of these conditions are equivalent. The coefficient of X_{33}^2 is a quadratic function in M_f and is always positive if the constant term $(M_eR_s)^2>0$ (obviously true), and if the discriminant is less than zero. The discriminant is

$$4(M_eM_g)^2 - 4(R_sM_e)^2 < 0$$

or

$$R_s^2 > M_g^2.$$

On substituting for M_g from Appendix II, the requirement that gain sensitivity decrease reduces to the following restriction on the load resistance:

$$R_l < R_s(2\omega_{30}/\omega_{20} - 1). \tag{8}$$

This expression, being independent of X_{33}, merely determines the boundary where gain sensitivity can always be improved. The amount of improvement is found from (7).

V. Effects of X_{33} on Gain–Bandwidth Product

The gain–bandwidth product is defined as the product of the square root of the transducer power gain and the fractional bandwidth of the LSUC. When $|X_{33}| = \infty$, gain–bandwidth product can be optimized [1]. For a given design this parameter can be calculated as a function of X_{33} by allowing $S_2\neq 0$, assuming X_{33} is a single-tuned lumped reactance, and calculating the gain (4) as a function of frequency when X_{33} is the desired reactance at midband. Using the same LSUC parameters defined in Table I, the gain–bandwidth product was calculated and plotted in Fig. 9 for the passive tuning case. For hot tuning and for $S_2=0$, the gain–bandwidth product is not changed enough to be seen on the scale of this graph.

The behavior of the gain–bandwidth product near $X_{33}=0$ needs some explanation. When $X_{33}\lesssim 0$, the gain is low and bandwidth wide, so values for the product are difficult to obtain. When $X_{33}\gtrsim 0$, the gain versus frequency curve has a large dip near the resonant point. For values of X_{33} in this range the maximum gain occurs at a frequency above resonance and the bandwidth is greatly reduced, making the gain–bandwidth product low.

VI. Effects of X_{33} on Noise Figure

From the various definitions for noise figure, the "actual noise figure" proposed by Kurokawa [9] is the most meaningful and the most convenient for negative-resistance amplifiers and converters. This definition includes the noise contribution from the load, so that two amplifiers which are not necessarily optimally loaded may be compared. The actual noise figure for an LSUC is defined as

$$F_2 = \frac{\text{noise power delivered to the load at } \omega_2}{\text{available noise input power at } \omega_1} \cdot \frac{1}{G_{21}}.$$

The noise power delivered to the load can be divided into three components: 1) noise from sources R_g+R_s at ω_1 and R_s at ω_3; 2) noise from internal sources of the up-converter at ω_2; and 3) noise from the load itself, which is amplified and returned to the load. The first noise component is

$$N_1 = 4kTBR_l\{(R_s + R_g)|Y_{21}|^2 + R_s|Y_{23}|^2\}$$

where k is Boltzmann's constant, T is the absolute temperature, and B is the bandwidth. The second component is assumed to come from R_s alone:

$$N_2 = 4kTBR_l|Y_{22}|^2R_s.$$

The third component is obtained by multiplying the output reflection gain of the amplifier by the available noise of the load.

$$N_3 = kTB \left| \frac{R_l - [(Y_{22})^{-1} - R_l]}{R_l + [(Y_{22})^{-1} - R_l]} \right|^2 = kTB \left| 1 - 2R_l Y_{22} \right|^2.$$

The sum of these three contributions gives the total noise power N, from which the actual noise figure is obtained:

$$F_2 = \frac{N}{kTBG_{21}} = 1 + \frac{R_s}{R_g} + \frac{4R_lR_s(|Y_{22}|^2 + |Y_{23}|^2)}{G_{21}} + \frac{|1 - 2R_lY_{22}|^2}{G_{21}}. \quad (9)$$

After some algebraic manipulation, the noise figure may be written as

$$F_2 = 1 + \frac{R_s}{R_g} + \frac{M_x + M_yX_{33} + M_zX_{33}^2}{(X_{31}X_{23} + X_{21}X_{33})^2 + (R_sX_{21})^2} \quad (10)$$

where M_x, M_y, and M_z are independent of X_{33} and are given in Appendix III. The minimum and maximum noise figure as a function of X_{33} can be found by differentiation. When $S_2=0$, i.e., $X_{23}=X_{32}=0$, the noise figure has only the one extremum at $X_{33}=0$. When $|X_{33}| = \infty$ as well, (10) reduces to

$$F_2 = \left(1 + \frac{R_s}{R_g}\right)\left(1 + \frac{\omega_{10}}{\omega_{20}}\right) + \frac{1}{G_{21}} \quad (11)$$

which can be minimized with respect to R_g, R_l, and ω_{20}/ω_{10} for a specified gain [1].

When $S_2=0$ but X_{33} is finite

$$F_2 = \left(1 + \frac{R_s}{R_g}\right)\left(1 + \frac{\omega_{10}}{\omega_{20}}\right) + \frac{1}{G_{21}} + \frac{R_sX_{13}(X_{13} + X_{31}\omega_{10}/\omega_{20})}{R_g(R_s^2 + X_{33}^2)}. \quad (12)$$

Comparison of (11) with (12) shows the noise figure increases as $|X_{33}|$ decreases and reaches a maximum when $X_{33}=0$, when there is no second-harmonic pump power. However, when $S_2 \neq 0$ there are two extrema of (10), and some improvement in noise figure is possible when X_{33} is finite. Using the LSUC parameters defined in Table I, the noise figure extrema are

$$X_{33} = -0.48\,\Omega \quad F_2 = 1.812 \quad \text{(maximum noise)}$$
$$X_{33} = 24.50\,\Omega \quad F_2 = 1.145 \quad \text{(minimum noise)}$$
$$|X_{33}| = \infty \quad F_2 = 1.146.$$

These extrema are plotted in Fig. 10 for various values of second-harmonic pumping. Minimum noise performance can be improved slightly by increasing S_2. The values of X_{33} for the gain and noise extrema are compared in Table II where it is shown that increasing the second-harmonic elastance component of the pumped varactor diode decreases the upper sideband reactance where these extrema occur.

VII. Conclusions

A low impedance path at the upper sideband frequency exerts a major influence on the performance of an LSUC. Furthermore, when an appreciable second-harmonic elastance coefficient exists, larger maximum gain and lower minimum noise figures are possible with fixed load and source impedance levels. Enhancement of S_2/S_0 moves the extrema to lower X_{33} values as shown using the LSUC parameters of Table I. This LSUC is most affected when $|X_{33}| \lesssim 20$.

The large discrepancy in gain, gain sensitivity, gain-bandwidth product, and noise figure between the cases when $|X_{33}| = \infty$ and when X_{33} is finite illustrates the need to consider the upper sideband circuit in the analysis of practical LSUC's. Over the range of X_{33}, the ratio of maximum-to-minimum midband gain can change as much as 13–21 dB (depending on S_2/S_0) with a corresponding change in noise figure from 1.1 to 1.9. An improvement in gain sensitivity to variation in the first-harmonic elastance coefficient S_1 is possible, although at the expense of reduced gain. When gain and X_{33} are specified, improved gain sensitivity can be guaranteed by appropriate choice of output load resistance and up-converter frequencies

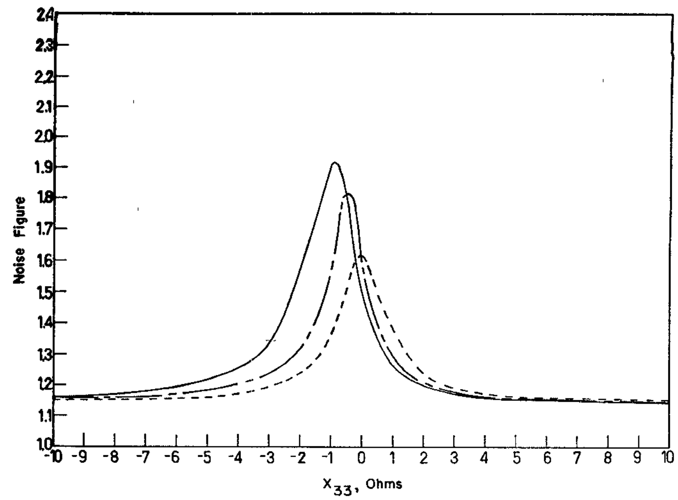

Fig. 10. Noise figure of LSUC of Table I where $S_2/S_0=0$ (----), $S_2/S_0=0.044$ (— —), and $S_2/S_0=0.1$ (——).

TABLE II
Values of X_{33} Where the Gain and Noise-Figure Extrema Occur for the LSUC of Table I

	$S_2=0$	$S_2/S_0=0.044$	$S_2/S_0=0.1$
Maximum gain	∞ Ω	9.77 Ω	5.62 Ω
Minimum gain	0 Ω	−0.538 Ω	−1.151 Ω
Minimum noise figure	∞ Ω	24.50 Ω	15.19 Ω
Maximum noise figure	0 Ω	−0.480 Ω	−1.062 Ω

Appendix I

The general expression for transducer power gain is given in (4). At midband where S_0 is resonated by appropriate circuit reactance, (4) can be expanded to show explicitly how the upper sideband power affects the power gain:

$$G_{21} = 4R_gR_l \frac{(X_{23}X_{31} + X_{21}X_{33})^2 + (R_sX_{21})^2}{M_a + (X_{33}M_b - M_c)^2} \quad (13)$$

where

$$M_a = [(R_g + R_s)(R_l + R_s)R_s - (R_g + R_s)X_{23}X_{32} + (R_l + R_s)X_{13}X_{31} - R_sX_{12}X_{21}]^2$$
$$M_b = (R_g + R_s)(R_l + R_s) - X_{12}X_{21}$$
$$M_c = X_{21}X_{13}X_{32} + X_{23}X_{31}X_{12}.$$

The maximum and minimum gain can be found by differentiating (13) with respect to X_{33}. The resulting quadratic equation

$$X_{33}^2(-M_bM_cX_{21}^2 - M_b^2X_{23}X_{31}X_{21}) - X_{33}[-M_dX_{21}^2 + (M_bX_{23}X_{31})^2 + (M_bR_sX_{21})^2] + M_dX_{23}X_{31}X_{21} + M_cM_b(X_{23}X_{31})^2 + M_bM_c(R_sX_{21})^2 = 0 \quad (14)$$

can be easily solved to find the desired gain extrema. In this equation $M_d = M_a + M_c^2$.

Appendix II

The midband gain sensitivity to variations in pump power given in (6) and (7) is obtained from the gain expression (5) where $S_2 = 0$. The factors used in (7) are

$$M_e = (R_g + R_s)(R_l + R_s) - S_1^2/(\omega_{10}\omega_{20})$$

$$M_f = (R_g + R_s)(R_l + R_s)R_s + (R_l + R_s)S_1^2/(\omega_{10}\omega_{30}) - R_sS_1^2/(\omega_{10}\omega_{20})$$

$$M_g = R_s - (R_l + R_s)\omega_{20}/\omega_{30}.$$

Appendix III

The parameters for the noise figure given in (10) are

$$M_x = \left(1 + \frac{R_s}{R_g}\right) X_{12}X_{21}R_s^2 + \frac{R_s}{R_g}[X_{23}^2(R_g + R_s)^2 + (X_{21}X_{13})^2 + X_{13}X_{31}X_{12}X_{21}] + \left(1 + \frac{R_s}{R_g}\right) \cdot [X_{23}X_{32}R_s(R_g + R_s) + X_{23}X_{32}X_{13}X_{31}] + \{[(R_g + R_s)(R_l + R_s)R_s - (R_g + R_s)X_{23}X_{32} + (R_l + R_s)X_{13}X_{31} + R_sX_{12}X_{21}]^2 + [X_{21}X_{13}X_{32} + X_{23}X_{31}X_{12}]^2\}/(4R_lR_g)$$

$$M_y = \left(1 + \frac{R_s}{R_g}\right)(X_{12}X_{23}X_{31} + X_{21}X_{13}X_{32}) - 2(X_{21}X_{13}X_{32} + X_{23}X_{31}X_{12})[(R_g + R_s)(R_l + R_s) - X_{12}X_{21}]/(4R_gR_l)$$

$$M_z = \left(1 + \frac{R_s}{R_g}\right) X_{12}X_{21} + [(R_g + R_s)(R_l + R_s) - X_{12}X_{21}]^2/(4R_gR_l).$$

Differentiating (10) with respect to X_{33} results in the following quadratic equation in X_{33}:

$$0 = X_{33}^2[-M_yX_{21}^2 + 2M_zX_{31}X_{23}X_{21}] + X_{33}[2M_z(X_{31}X_{23})^2 + 2M_z(X_{21}R_s)^2 - 2M_xX_{21}^2] + [M_y(X_{31}X_{23})^2 + M_y(X_{21}R_s)^2 - 2M_xX_{21}X_{31}X_{23}]$$

which can be easily solved to obtain the noise figure extrema.

References

[1] P. J. Khan, "Optimum design of low-noise lower sideband parametric up-converters," *IEEE Trans. Electron Devices*, vol. ED-18, pp. 924–931, Oct. 1971.

[2] J. A. Luksch, E. W. Matthews, and G. A. VerWys, "Design and operation of four-frequency parametric up-converters," *IRE Trans. Microwave Theory Tech.*, vol. MTT-9, pp. 44–52, Jan. 1961.

[3] D. B. Anderson and J. C. Aukland, "Transmission-phase relations of four-frequency parametric devices," *IRE Trans. Microwave Theory Tech.*, vol. MTT-9, pp. 491–498, Nov. 1961.

[4] A. Korpel and V. Ramaswamy, "Input conductance of four-frequency parametric up-converter," *IEEE Trans. Microwave Theory Tech.*, vol. MTT-13, pp. 96–106, Jan. 1965.

[5] R. L. Ernst, "Multiple-idler parametric amplifiers," *IEEE Trans. Microwave Theory Tech.*, vol. MTT-15, pp. 9–22, Jan. 1967.

[6] D. P. Howson and R. B. Smith, *Parametric Amplifiers*. London, England: McGraw-Hill, 1970, ch. 6.

[7] B. J. Robinson, "Theory of variable-capacitance parametric amplifiers," *Proc. Inst. Elec. Eng.*, Mono 480E, Nov. 1961.

[8] P. J. Khan, "Parametric amplifier nonresonant gain maximum," *Proc. IEEE* (Lett.), vol. 56, pp. 99–100, Jan. 1968.

[9] K. Kurokawa, "Actual noise measure of linear amplifiers," *Proc. IRE*, vol. 49, pp. 1391–1397, Sept. 1961.

General Field Theory Treatment of *H*-Plane Waveguide Junction Circulators

M. EZZAT EL-SHANDWILY, AHMAD A. KAMAL, AND ESMAT A. F. ABDALLAH

***Abstract*—In this paper an exact field theory treatment for the waveguide junction circulators is presented. The treatment is general, being dependent on neither the geometrical symmetry of the junction nor the number of ports. The electromagnetic fields in the joining waveguides are written in the form of infinite summation of waveguide modes. The solutions of the wave equations in the ferrite rod and in the surrounding air are obtained in the form of infinite summation of cylindrical modes. The fields at the ferrite air interface and at an imaginary boundary chosen arbitrarily between the air region and the waveguides are then matched. This process leads to an infinite system of nonhomogeneous equations in the field amplitudes.**

Three types of waveguide junction circulators using this technique are analyzed: the simple ferrite-rod Y junction, the simple ferrite-rod T junction, and the latching Y junction.

Point-matching techniques are used to get numerical results for the field distributions and the circulator characteristics. Excellent agreement has been found between the published experimental measurements and the numerical results obtained by this technique.

Manuscript received August 25, 1972; revised December 13, 1972.

M. E. El-Shandwily and E. A. F. Abdallah are with the Electrical and Electronic Engineering Laboratory, National Research Centre, Dokki, Cairo, Egypt.

A. A. Kamal is with the Department of Electronic and Communication Engineering, Faculty of Engineering, Cairo University, Cairo, Egypt.